Modeling of damage in ductile cast iron - The effect of including plasticity in the graphite nodules

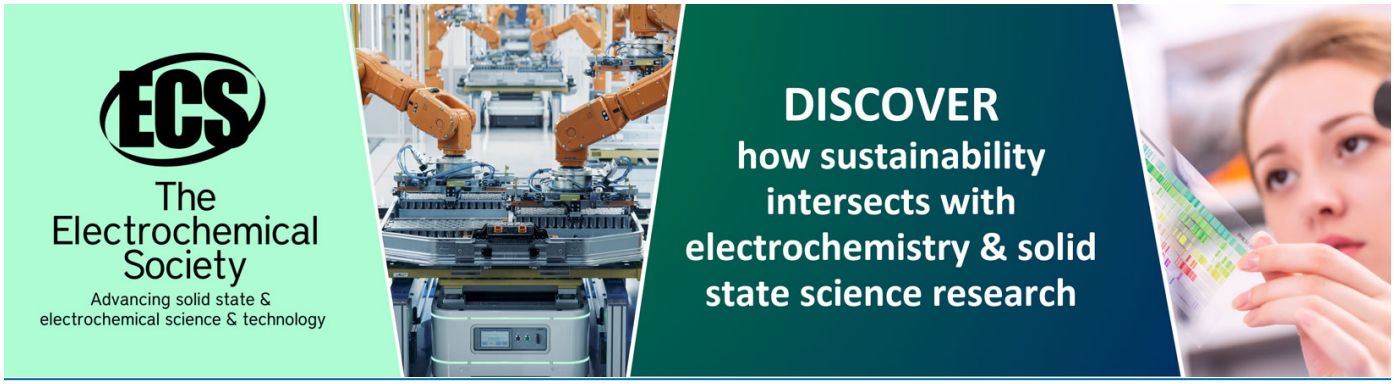

Modeling of damage in ductile cast iron – The effect of including plasticity in the graphite nodules

T Andriollo[1], J Thorborg[2], N S Tiedje[1] and J Hattel[1]
[1]Department of Mechanical Engineering, Technical University of Denmark, DK-2800 Kgs. Lyngby, Denmark
[2]MAGMA GmbH, D-52072 Aachen, Germany

E-mail: titoan@mek.dtu.dk

Abstract. In the present paper a micro-mechanical model for investigating the stress-strain relation of ductile cast iron subjected to simple loading conditions is presented. The model is based on a unit cell containing a single spherical graphite nodule embedded in a uniform ferritic matrix, under the assumption of infinitesimal strains and plane-stress conditions. Despite the latter being a limitation with respect to full 3D models, it allows a direct comparison with experimental investigations of damage evolution on the surface of ductile cast iron components, where the stress state is biaxial in nature. In contrast to previous works on the subject, the material behaviour in both matrix and nodule is assumed to be elasto-plastic, described by the classical J2-flow theory of plasticity, and damage evolution in the matrix is taken into account via Lemaitre's isotropic model. The effects of residual stresses due to the cooling process during manufacturing are also considered. Numerical solutions are obtained using an in-house developed finite element code; proper comparison with literature in the field is given.

1. Introduction

Since its commercial introduction in 1948, ductile cast iron (DCI) has constantly found new fields of application, ranging from the automotive sector to the wind power industry. Castings made of DCI are especially attractive as they combine high ductility and strength together with lower price compared to traditional low carbon steel. Surprisingly, despite extensive experimental work carried out in the last 60 years [1], little has been done to cast light on the microscopic features which determine the constitutive behavior of the material at the macroscopic scale.

In some papers published in literature in the 90's, DCI has been assumed to behave as a porous material [2][3][4], in consideration to the "soft" nature of the graphite and the weak strength of the nodule-matrix interface, for which the Gurson-Tvergaard-Needleman model reasonably applies [5].

On the other side, in the last decade several researchers have pointed out that some effects observed during deformation of DCI cannot be explained by a simple voided-matrix material model. First of all, it has been proved that fatigue in DCI cannot be analyzed using a linear elastic fracture mechanics framework [2]; this might be related to the fact that, according to the imposed stress intensity factor, different competing damage mechanisms seem to be active in the matrix and/or in the nodule [6]. Moreover, tensile and compression tests of DCI samples conducted at different temperatures have highlighted large differences in the deformed nodule shapes [7]: if the nodule stiffness and strength were negligible compared to the matrix in the entire range of temperatures considered, the graphite

Nomenclature

$\bar{\varepsilon}_{ij}$	Volume average of total strain tensor	D	Damage variable
$\bar{\varepsilon}_{ij}$	Volume average of total strain tensor	$S,\ s$	Lemaitre's damage evolution parameters
$\bar{\sigma}_{ij}$	Volume average of the stress tensor	Y	Energy release rate
R_v	Triaxiality function	f	Yield function
s_{ij}	Deviatoric part of the stress tensor	$k,\ n$	Isotropic hardening parameters
δ_{ij}	Kronecker delta	p	Equivalent Von Mises plastic strain
$\varepsilon_{ij}^{tot},\ \varepsilon_{ij}^{e},\ \varepsilon_{ij}^{p}$	Total/elastic /plastic strain tensor	p_{crit}	Critical effective plastic strain for damage evolution
σ_{ij}	Stress tensor		
σ_e	Equivalent Von Mises stress	r	Hardening variable
$\sigma_y,\ \sigma_y^0$	Actual / initial yield stress	α	Thermal expansion coefficient
E	Young's modulus	λ	Plastic multiplier
E^T	Tangent modulus	ν	Poisson's ratio

should always deform in the same manner. Finally, the almost continuous variation of the DCI Young's modulus with respect to strain in the very early deformation range [8] can hardly be explained by plasticity induced only by the presence of spherical voids.

Recently, Bonora & Ruggiero [9] have drawn attention to the role played by residual stresses which develop during the cooling phase of the manufacturing process as a result of the thermal expansion coefficient mismatch between the matrix and the graphite nodules. In their work, the constitutive response of a ferritic DCI has been numerically simulated using a micromechanical approach based on a 2D axisymmetric unit cell, assuming linear elastic behavior of the graphite and allowing plasticity together with damage evolution in the metallic matrix.

The present work extends the findings of Bonora & Ruggiero by investigating the influence of graphite stiffness and yield strength on the elastic parameters of ferritic DCI during tensile uniaxial testing. Special focus is put on explaining how inelastic deformation induced by the combined action of residual stresses and external loading affects the material response in the early deformation range.

2. Micromechanical model

Microscopic observations of local deformation and damage evolution in cast irons are taken, in most of the cases, on the surface of the component under examination [10][11][12], where the stress state is biaxial in nature. In order to produce results which are closely comparable with experimental findings, a 2D micromechanical model subjected to plane-stress conditions is developed. Graphite nodules are assumed to be spheres of equal size homogeneously dispersed in the ferritic matrix; the DCI microstructure is therefore schematized as a periodic square unit cell with a central circular graphite nodule (figure 1). The ratio between nodule radius and cell side is taken to be 0.39; this gives a graphite area fraction of approximately 12%, corresponding to the graphite volume fraction typical of GJS 400-18 according to EN 1563 ferritic DCI [4], which will be considered as reference material throughout the analysis.

Because of symmetry considerations, only ¼ of the unit cell is analyzed (figure 2). Periodic boundary conditions are applied in order to generate axial normal loading, yet fulfilling continuity of displacement and surface tractions along the cell boundaries, as discussed in [13]. Following Bonora & Ruggiero, the nodule-matrix transition is modelled as a frictionless contact interface, without any tensile strength in the normal direction, i.e. only compressive normal stresses can be transmitted across the interface. The mesoscopic Young's modulus E_{DCI} for the periodic unit cell is defined as:

$$E_{DCI} = \lim_{\bar{\varepsilon}_{11}\to 0}\left(\frac{\partial\bar{\sigma}_{11}}{\partial\bar{\varepsilon}_{11}}\right) \tag{1}$$

where $\bar{\sigma}_{11}$, $\bar{\varepsilon}_{11}$ and $\bar{\varepsilon}_{22}$ denote normal components of the mesoscopic stress and strain, given by the average over the unit cell volume of the corresponding microscopic quantities.

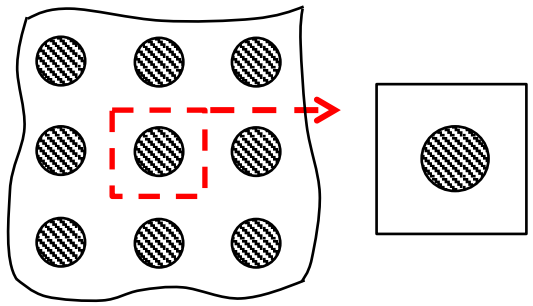

Figure 1. Assumed DCI microstructure, with identification of the periodic unit cell.

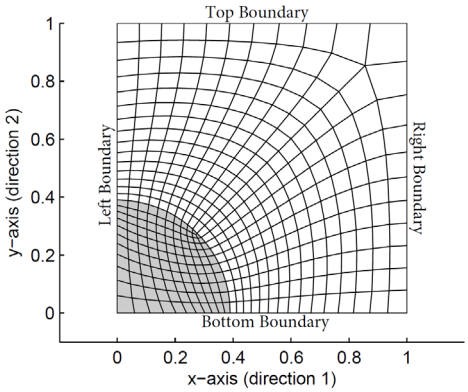

Figure 2. View of 2D mesh of ¼ of the periodic unit cell.

3. Constituents material behavior

3.1. Ferritic matrix

In light of its soft ductile nature, the constitutive behavior of the ferritic matrix is assumed to be described by the isotropic Lemaitre's damage model [14], whose basic equations in Cartesian components are summarized as follows:

- additive strain decomposition:

$$\varepsilon_{ij}^{tot} = \varepsilon_{ij}^{e} + \varepsilon_{ij}^{p} + \delta_{ij}\alpha\Delta T \tag{2}$$

- elastic constitutive law:

$$\frac{\sigma_{ij}}{1\text{-}D} = \frac{E}{1+\nu}\left[\varepsilon_{ij}^{e} + \frac{\nu}{1\text{-}2\nu}\delta_{ij}\varepsilon_{kk}^{e}\right] \tag{3}$$

- flow rule:

$$\dot{\varepsilon}_{ij}^{p} = \frac{3s_{ij}}{2\sigma_e}\frac{\dot{\lambda}}{1\text{-}D} \tag{4}$$

- yield function:

$$\mathrm{f} = \frac{\sigma_e}{1\text{-}D} - \sigma_y(\mathrm{r}) \le 0, \qquad \sigma_e = \left(\frac{3}{2}s_{ij}s_{ij}\right)^{1/2} \tag{5}$$

- isotropic hardening rule:

$$\sigma_y = k(r+r_0)^n, \qquad r_0 = \left(\frac{\sigma_y^0}{k}\right)^{1/n} \tag{6}$$

- effective plastic strain increment and hardening parameter increment:

$$\dot{p} = \frac{\dot{r}}{1\text{-}D}, \qquad \dot{r} = \dot{\lambda} \tag{7}$$

- damage evolution law:

$$\dot{D} = \left(\frac{Y}{S}\right)^{s}\dot{p}, \qquad \text{if } p > p_{crit} \tag{8}$$

- energy release rate:

$$\mathrm{Y} = \frac{\sigma_e^2 R_v}{2E(1\text{-}D)^2}, \qquad R_v = \frac{2}{3}(1+\nu) + 3(1\text{-}2\nu)\left(\frac{\sigma_{kk}}{3\sigma_e}\right)^2 \tag{9}$$

- consistency condition:

$$\mathrm{f} \le 0, \qquad \dot{\lambda} \ge 0, \qquad \mathrm{f}\dot{\lambda} = 0 \tag{10}$$

It may be noticed that knowledge of 9 material parameters is required: 3 thermo-elastic (E,ν,α), 3 related to plastic flow (σ_y^0,k,n) and finally 3 related to damage (p_{crit},S,s). In principle, an additional parameter specifying the conditions at which crack nucleation occurs would be necessary: however, in the present analyses damage never exceeds 0.1, which is well below the critical fracture initiation threshold for common metals and alloys.

Values for Young's modulus, linear thermal expansion coefficient and initial yield stress, together with their temperature dependence, are reported in table 1; regarding Poisson's ratio, a constant value of 0.3 is assumed [15]. The remaining five parameters to be entered in the model have been determined on the basis of a data-fitting optimization procedure [16], minimizing the error between the predicted numerical results and the reference uniaxial stress-strain curve at room temperature for ferrite reported in [15]. Calculated values are given in table 2.

As no information is available for the post-yielding behavior of the ferritic matrix at higher temperatures, plastic flow and damage evolution parameters are assumed to be constant, except for the temperature dependence of the initial yield stress previously mentioned. Time-dependent deformation mechanisms are also neglected.

Table 1. Material properties for ferritic matrix (after Bonora & Ruggiero [9]).

Temperature (°C)	Young's modulus (GPa)	Thermal exp. coefficient ($x10^{-5}$ °C^{-1})	Initial yield stress (MPa)
25	210.0	1.25	297
250	153.8	1.50	194
500	102.5	1.60	137
750	41.4	-	96
900	20.0	-	70
1000	0.1	2.40	60

Table 2. Plastic flow and damage evolution parameters for ferritic matrix.

Plastic flow factor k (MPa)	Plastic flow exponent n	Damage factor S (MPa)	Damage exponent s	Critical eff. plastic strain p_{crit} (mm/mm)
818.0	0.245	0.357	0.167	$5.33x10^{-3}$

3.2. Graphite nodules

As correctly pointed out by Bonora & Ruggiero, very little has been published in literature regarding the mechanical behavior of DCI nodules. At present, available mechanical data come mainly from nano-indentation measurements, which have provided values for Young's modulus in the range 15 GPa [10] to 28 GPa [17]; however, such numbers are not in agreement with Bonora & Ruggiero's numerical findings, who have proposed much higher stiffness values, in the order of 300-375 GPa.

In the present work, the graphite nodules are assumed to follow a linear elastic-perfectly plastic behavior described by the classical J2-flow theory of plasticity, and different values of Young's modulus and yield strength are considered in order to assess the related effects on the constitutive response of the entire unit cell. Poisson's ratio and linear thermal expansion coefficient are assumed to be 0.15 and $2.5x10^{-6}$ °C^{-1} respectively; no temperature dependence of any material parameter is taken into consideration.

4. Finite element modeling and simulations setup

The mechanical behavior of the unit cell is investigated by means of an "in-house" developed implicit FE C-code based on a small strains formulation. The mesh, shown in figure 2, is composed by 4-node isoparametric plane-stress quadrilateral elements with full integration. The nodule-matrix contact interface is modeled using a penalty-based method in association with an isoparametric discretization based on shape functions [18]. Non-linearity, arising from the constituent's material behavior and the contact condition, is numerically handled by means of a full Newton-Raphson scheme in combination

with an implicit elastic predictor-return mapping algorithm [19]. For the purpose of improving convergence, a suitable expression for the consistent tangent modulus in the special case of plane stress and isotropic Lemaitre's damage model is derived and implemented in the code.

Numerical analyses are performed by initially applying a uniform temperature decrease to the entire cell, from 1000 °C down to room temperature, in order to simulate the cooling stage during manufacturing of ferritic DCI, in agreement with the considerations reported by Bonora & Ruggiero. Subsequently, a mesoscopic strain $\bar{\varepsilon}_{11}$ of $5\text{x}10^{-3}$ is progressively imposed to investigate the unit cell behavior during uniaxial tension.

A first set of simulations is run by varying the graphite Young's modulus in the range 1 to 500 GPa, while keeping its yield strength very high, which is equivalent to assuming linear elastic behavior of the nodules. Then, the graphite Young's modulus is kept fixed at selected values and tests are performed for graphite yield strength $\sigma_{y,g}$ in the interval 10 to 500 MPa. An additional simulation with "zero" graphite stiffness is also carried out, in order to have a direct comparison with the voided-matrix model mentioned in the introduction.

5. Results

5.1. Effect of graphite Young's modulus

In this section, the outcome of the numerical analyses focusing on the influence exerted by the nodules stiffness on the unit cell constitutive response in the early deformation range is presented, under the assumption of infinite graphite yield strength.

Figure 3 shows the obtained mesoscopic stress-strain tensile curve for selected values of E_g. The variation of the curve initial slope, which corresponds to the definition of the mesoscopic Young's modulus given in equation (1), is instead reported in figure 4. Starting from the voided matrix value corresponding to zero graphite stiffness, 3 different ranges may be identified: a first one in which E_{DCI} exhibits a small linear growth with E_g, a second one in which E_{DCI} drops abruptly to approximately 55 % of its initial value, and finally a third one in which E_{DCI} returns to increase, but not linearly. This particular behavior is related to the twofold effect played by an increase in the graphite stiffness: from one side, it makes the entire unit cell stiffer, as the nodule offers greater resistance to be deformed to a horizontal "oval" shape by the surrounding matrix during tensile loading; from the other side, it drives higher residual stresses at the end of the cooling stage, increasing the risk of promoting plastic deformation in the matrix, with consequent loss of stiffness.

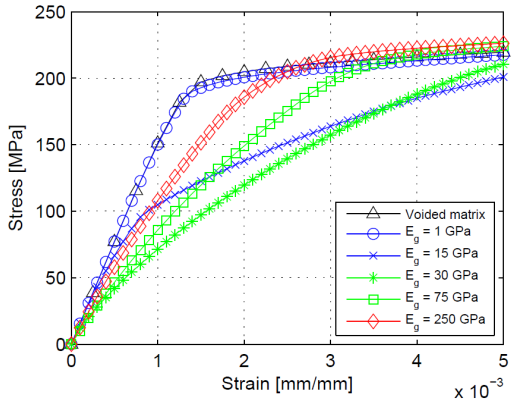

Figure 3. Mesoscopic tensile curves for selected values of the graphite Young's modulus.

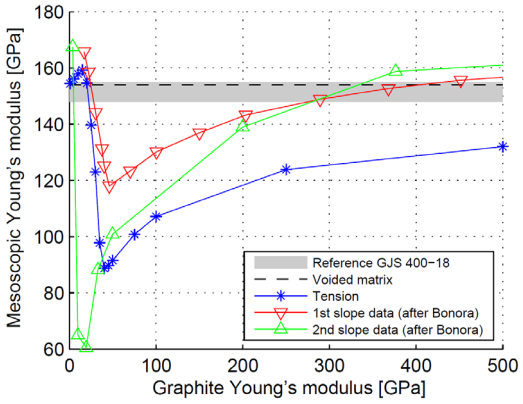

Figure 4. Calculated mesoscopic Young's modulus as a function of the graphite stiffness. Data are compared with findings from [9].

It is worth noticing that the shape of the calculated mesoscopic tensile stress-strain curves depicted in figure 3 closely matches the results reported by Bonora & Ruggiero in [9], figure 9; this is particularly evident when comparing the curves obtained for E_g = 15 GPa, which show exactly the same type of slope "break point" in the very early deformation range. This is indicative of the capacity of the two models to simulate the same physical mechanisms, despite Bonora & Ruggiero's analysis being based on a 2D axisymmetric cell coupled with a different damage formulation. Moreover, the mesoscopic Young's modulus evolution with E_g describes a pattern very similar to that of the "first slope" recorded by the two abovementioned authors, as shown in figure 4. Regarding this point, however, no comment is made in their paper about the initial linear elastic regime at very low E_g values, where an increment in the graphite Young's modulus produces a proportional increase in the global cell stiffness, the voided matrix value representing a lower bound.

5.2. Effect of graphite yield strength

The previous results have highlighted the fundamental role played by the residual stresses in determining the mechanical response of the unit cell in the early deformation range. However, it is likely that all analyses presented so far have somehow been biased by overestimating the amount of plasticity induced in the matrix by assuming infinitely high graphite yield strength $\sigma_{y,g}$. In order to investigate this point, the influence of nodule yielding on the predicted mesoscopic quantities is studied for two values of graphite Young's modulus: 15 and 300 GPa, which correspond to the literature values mentioned in section 3.2.

From a qualitative point of view, it is seen from figure 5 that very low graphite yield strength values provide mesoscopic tensile curves which are similar to that of the voided matrix. The reason is the following. During initial cooling the stress state in the nodule is homogeneous; therefore, the yield point is reached simultaneously on the whole area occupied by graphite. As perfect plasticity does not allow any hardening of the graphite, the stress state in the entire cell does not vary anymore during the remaining uniform temperature decrease; shrinkage of the matrix around the nodule is simply accommodated by plastic flow of the latter in the 3rd dimension. As a consequence, if the graphite yield strength is very low, the residual stress pattern in the matrix becomes "frozen" at the very beginning of the cooling process, when the magnitude of the stresses is still negligible. In addition, during subsequent tensile testing, the nodule opposes with very little resistance to deformation, again because of its very low yield strength.

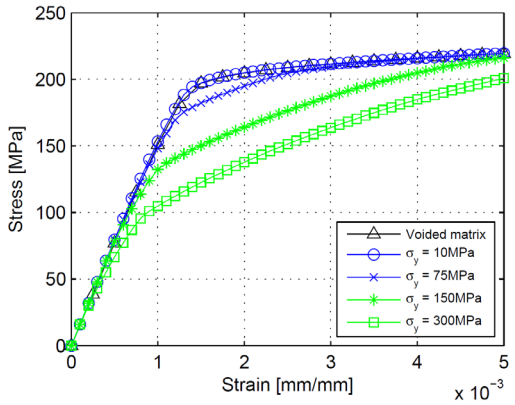

Figure 5. Mesoscopic tensile curves for selected values of the graphite yield strength, obtained using a graphite stiffness of 15 GPa.

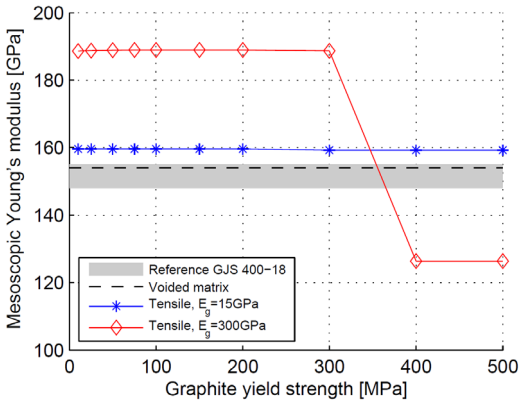

Figure 6. Calculated mesoscopic Young's modulus as a function of the graphite yield strength.

The above discussion leads to the conclusion that when the graphite yield strength is decreased, the unit cell tends to behave according to the voided matrix model, irrespective of the graphite stiffness.

Conversely, for sufficiently high values of $\sigma_{y,g}$, the nodule never yields during testing, and the mesoscopic tensile curves become the same as those reported in Figure 3: for instance, in figure 5 this happens for $\sigma_{y,g}$ equal to 300 MPa.

The effect of graphite yield strength on the mesoscopic Young's modulus is reported in figure 6. It may be observed that in the case with E_g = 15 GPa, the cell stiffness is almost independent of $\sigma_{y,g}$, and its value is slightly higher than that of the reference voided matrix. This is due to two things. First, as pointed out in section 5.1, such graphite stiffness is too low to produce any yielding in the matrix at the end of the cooling stage, even if plastic flow in the nodule is neglected. Moreover, when subsequent tensile loading begins, unloading takes place in the nodule, implying that "almost" the entire unit cell is the elastic regime, no matter the value of $\sigma_{y,g}$. In this situation, the presence of the nodule simply hinders lateral contraction of the matrix during tensile testing, increasing the mesoscopic cell stiffness.

It is interesting to notice that the same reasoning applies when E_g = 300 GPa, but only for values of the graphite yield strength below 300 MPa. In this case, yielding of the nodule prevents yielding of the matrix during cooling, which would otherwise take place. At the same time, the high elastic graphite stiffness leads to an exceptionally high value of the mesoscopic Young's modulus, which would never be achieved if plastic flow in the nodule was inhibited, as comparison between figure 6 and figure 4 demonstrates. In fact, as soon as $\sigma_{y,g}$ is increased beyond the critical threshold of approx. 400 MPa, matrix yielding at the end of initial cooling occurs and E_{DCI} reduces dramatically. Evidence of the fundamental role that graphite strength plays in determining the cell mesoscopic stiffness via affecting the plastic yielding distribution is given in figure 7 and figure 8.

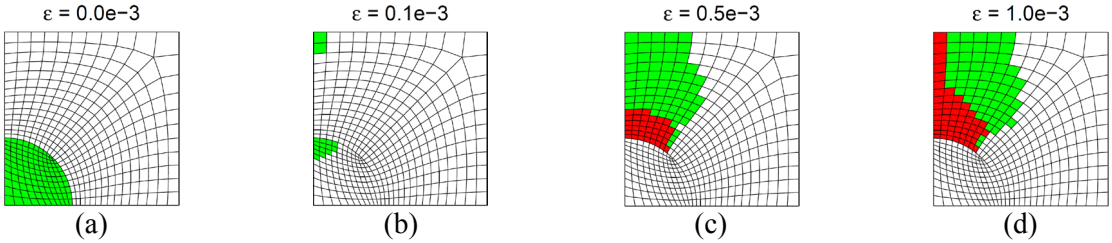

Figure 7. Plastic yielding (green) and damage (red) evolution at the beginning of tensile testing, for $\sigma_{y,g}$ = 300 MPa and E_g = 300 GPa. The mesoscopic strain level is indicated above each contour.

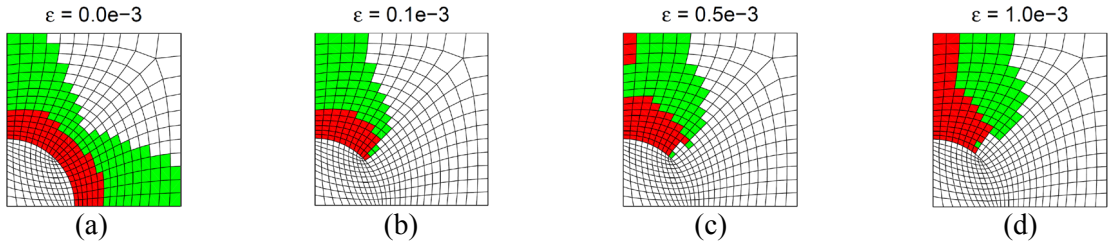

Figure 8. Plastic yielding (green) and damage (red) evolution at the beginning of tensile testing, for $\sigma_{y,g}$ = 400 MPa and E_g = 300 GPa. The mesoscopic strain level is indicated above each contour.

6. Conclusions

In the present paper a micromechanical model based on a 2D periodic unit cell subjected to plane-stress conditions has been used to investigate the ductile cast iron behavior in the early deformation range. The influence of graphite stiffness and strength on the mesoscopic "elastic" parameters have been analysed and discussed, extending and clarifying the findings obtained by Bonora & Ruggiero in a previous work. In particular, the mechanical response of the unit cell has proved to be strongly affected by the imposition of a threshold on the maximum load carrying capacity of the nodule.

According to the present results, very high graphite Young's modulus values, in the range of 300 to 400 GPa, are probably to be excluded. In fact, if the graphite yield strength is assumed to be finite and of reasonable values, yielding of the nodule would prevent matrix plastification during the initial cooling stage, thus leading to values of the mesoscopic stiffness above the admissible range. As a consequence, graphite Young's modulus values in the order of a few tens of GPa appear more sensible, in agreement with nano-indentation data reported in literature.

References

[1] Labrecque C and Gagne M 1998 Review ductile iron: 50 years of continuous development *Can. Metall. Q.* **37** 343–78
[2] Dong M J, Tie B, Béranger A S, Prioul C and François D 1997 Damage Effect on the Fracture Toughness of Nodular Cast Iron *Adv. Mater. Res.* **4-5** 181–8
[3] Berdin C, Dong M J and Prioul C 2001 Local approach of damage and fracture toughness for nodular cast iron *Eng. Fract. Mech.* **68** 1107–17
[4] Steglich D 1998 Micromechanical modeling of damage and fracture of ductile materials *Fatigue Fract. Eng. Mater. Struct.* **21** 1175–88
[5] Gurson A 1977 Continuum theory of ductile rupture by void nucleation and growth: Part 1 - Yield criteria and flow rules for porous ductile media *J. Eng. Mater. Technol. ASME* **99** 2 – 15
[6] Di Cocco V, Iacoviello F and Cavallini M 2010 Damaging micromechanisms characterization of a ferritic ductile cast iron *Eng. Fract. Mech.* **77** 2016–23
[7] Hervas I, Bettaieb M B and Hug E 2013 Damage mechanisms evolution of ductile cast irons under thermomechanical loadings *Int. J. Mater. Prod. Technol.* **47** 23
[8] Kohout J 2001 A simple relation for deviation of grey and nodular cast irons from Hooke's law *Mater. Sci. Eng. a* **A313** 16 – 23
[9] Bonora N and Ruggiero A 2005 Micromechanical modeling of ductile cast iron incorporating damage. Part I: Ferritic ductile cast iron *Int. J. Solids Struct.* **42** 1401–24
[10] Dierickx P, Verdu C, Reynaud A and Fougeres R 1996 A study of physico-chemical mechanisms responsible for damage of heat treated and as-cast ferritic spheroïdal graphite cast irons *Scr. Mater.* **34** 261–8
[11] Di Cocco V, Iacoviello F, Rossi A and Iacoviello D 2014 Macro and microscopical approach to the damaging micromechanisms analysis in a ferritic ductile cast iron *Theor. Appl. Fract. Mech.* **69** 26–33
[12] Sjögren T, Persson P E and Vomacka P 2010 Analysing the Deformation Behaviour of Compacted Graphite Cast Irons Using Digital Image Correlation Techniques *Key Eng. Mater.* **457** 470–5
[13] Drago A and Pindera M 2007 Micro-macromechanical analysis of heterogeneous materials: Macroscopically homogeneous vs periodic microstructures *Compos. Sci. Technol.* **67** 1243–63
[14] Lemaitre J 1985 A continuous damage mechanics model for ductile fracture *J. Eng. Mater. Technol. ASME* **107** 83 – 89
[15] Zhang K S, Bai J B and François D 1999 Ductile fracture of materials with high void volume fraction *Int. J. Solids Struct.* **36** 3407–25
[16] Lemaitre J and Desmorat R 2005 *Engineering damage mechanics : ductile, creep, fatigue and brittle failures* (Springer)
[17] Pradhan S K, Nayak B B, Sahay S S and Mishra B K 2009 Mechanical properties of graphite flakes and spherulites measured by nanoindentation *Carbon N. Y.* **47** 2290–2
[18] Wriggers P 2006 *Computational Contact Mechanics* (Springer)
[19] Neto E de S, Peric D and Owens D R J 2008 *Computational methods for plasticity : theory and applications* (Wiley)